Comparison among Slip-Link Simulations of Bidisperse Linear Polymer Melts

Yuichi Masubuchi,*,†,‡ Hiroshi Watanabe,† Giovanni Ianniruberto,§ Francesco Greco,|| and Giuseppe Marrucci§

Institute for Chemical Research, Kyoto University, Gokasyo, Uji, Kyoto 611-0011, Japan, Japan Science and Technology, Kyoto 611-0011, Japan, Dipartimento di Ingegneria Chimica, Università degli studi di Napoli "Federico II", Piazzale Tecchio 80, 80125 Napoli, Italy, and Istituto di Ricerche sulla Combustione − CNR, Piazzale Tecchio 80, 80125 Napoli, Italy

Received April 28, 2008; Revised Manuscript Received August 15, 2008

ABSTRACT: Recent simulations of entangled polymer dynamics are based on slip-link models pioneered by Hua and Schieber (*J. Chem. Phys.* **1998**, *109*, 10018). In this study, we compare different slip-link models in their prediction of the linear viscoelasticity of bidisperse linear polymers to examine how effectively such models account for constraint release. We compare the DT model by Doi and Takimoto (*Philos. Trans. R. Soc. London, Ser. A* **2003**, *361*, 641), the NS model by Nair and Schieber (*Macromolecules* **2006**, *39*, 3386), and the primitive chain network (PCN) model by Masubuchi et al. (*J. Chem. Phys.* **2001**, *115*, 4387). It is found that DT and PCN models are in better quantitative agreement with literature data than is the NS model. This indicates that renewal of entanglements along the chain due to constraint release, explicitly accounted for in DT and PCN, is not equivalent to spatial fluctuations of slip-links, as included in the NS mean field approach.

Introduction

In recent times, slip-link simulations (pioneered by Hua and Schieber[1]) have been developed to describe entangled polymer dynamics. They represent a sort of combination of the temporary network model[2] and the reptation model.[3] In the simulations, a network consisting of nodes (slip-links) and elastic segments (standing for entanglements and polymer subchains, respectively) replaces the actual entangled polymers. Because of the longitudinal diffusion of the polymers along their primitive paths, the molecular weight of the strands and even the number of strands fluctuate in time. In their turn, also the network node positions change in time because of convection and, possibly, because of fluctuations. Therefore, the state variables of the system describing such a behavior are the position of the network nodes, $\{\mathbf{R}\}$, the monomer number in each network strand or chain segment, $\{n\}$, and the number of segments per chain, $\{Z\}$.

In the Hua−Schieber model,[1] the network is described as an ensemble of unconnected primitive chains, each composed of Z successive segments, embedded in the medium. Hence, $\{\mathbf{R}\}$ moves affinely with the macroscopic deformation. Time evolution of $\{n\}$ is calculated by a one-dimensional diffusion equation describing the sliding motion of a bead-spring chain along its contour. In such equation, drag and elastic forces are considered as well as random forces due to thermal agitation. Change in $\{Z\}$ arises by creation and destruction of slip-links next to chain ends. When the segment length at a chain end becomes zero due to the sliding motion of the chain, the slip-link is removed. On the contrary, when the chain-end length exceeds a certain critical value, a new slip-link is created at some point along the last segment, and the tangent vector of the new end segment is assigned randomly. Because it is well-known that also constraint release due to reptation and fluctuation of surrounding chains is a significant relaxation mechanism,[4] some coupling between network nodes is introduced so as to account for constraint release. Specifically, when at a chain end a node happens to be removed, another node on another chain is randomly selected and the creation times of these two nodes are compared. Next, also the selected node is removed, but only if its creation time precedes that of the removed node.

Following the framework of the HS model, several different models[5−9] have been proposed with different rules for the time evolution of the state variables, and all such models reproduce almost quantitatively the linear viscoelastic data of monodisperse linear polymers, thus confirming the validity of depicting entanglements as slip-links, which is the common feature of all those models. However, no analysis has ever been made of the effect of the different assumptions incorporated in the models, specifically on those aspects of the kinetics of $\{Z\}$ and/or $\{\mathbf{R}\}$ somehow describing constraint renewal. Now because it is expected that constraint renewal does not significantly affect the linear behavior of monodisperse linear polymers, another benchmark situation must be looked for to check those assumptions.

A possible critical test might be the dynamics of bidisperse linear polymers (blends of short and long chains). Many studies have been reported for bidisperse blends following the work of Tsenoglou[10] and des Cloizeaux.[11] They derived mixing rules for the linear viscoelasticity of polydisperse systems on the basis of the idea of double reptation, a simplified version of constraint release. Molecular theories relating constraint release to chain dynamics in the tube were then developed,[12−17] most of them giving the overall relaxation as a product of two functions, one describing reptation, the other constraint release dynamics.

One of the main motivations to introduce slip-links is to account in a direct way for the coupling between constraint release and chain relaxation. However, on bidisperse linear polymers, only a few slip-link simulation results have so far been reported,[9] and the problem still appears open. Indeed, Hua and Ke[18] mention that some slip-link simulations could not predict bidisperse melt dynamics.

Slip-link models account for constraint release by change in either $\{\mathbf{R}\}$,[9] or in both $\{\mathbf{R}\}$ and $\{Z\}$.[5,6] Change in $\{\mathbf{R}\}$ alone due to constraint renewal corresponds to the mechanism referred

* To whom correspondence should be addressed. Phone: +81-774-38-3136. Fax: +81-774-38-3139. E-mail: mas@scl.kyoto-u.ac.jp.
† Kyoto University.
‡ Japan Science and Technology.
§ Università degli studi di Napoli "Federico II".
|| Istituto di Ricerche sulla Combustione − CNR.

10.1021/ma800954q CCC: $40.75
Published on Web 10/08/2008

to as constraint release Rouse dynamics (CR-Rouse).[4,20] In such a picture, the "tube", or equivalently the set of slip-links of a chain, undergoes a Rouse-like motion because at each constraint removal the chain makes a local jump before getting entangled again with some other chain (hence Z does not change, but only $\mathbf{R}$). Change of both $\mathbf{R}$ and Z occurs when the slip-link is actually removed because of sliding away of the partner chain; hence there is an explicit Z dynamics due to motion of other chains. The latter can also introduce new entanglements in the test chain. However, when the dynamics of some of the surrounding chains is much faster than the slow dynamics of the test chain, the corresponding entanglements are not effective. Such a reduction in the effective Z due to the high blinking frequency of some topological constraints (an increase of the effective tube diameter) is referred to as dynamic tube dilation (DTD).[19] In the DTD picture, entanglement segments are progressively coarse grained during relaxation; that is, the size of the effective tube segment increases in time as a result of constraint renewal by the surrounding chains.

Watanabe et al.[21,22] maintained that, because DTD requires equilibration of the coarse-grained segment, and such equilibration event occurs over the appropriate relaxation time, DTD and CR-Rouse occur in competition. In the short time region, coarse-graining (DTD) prevails because the CR-Rouse relaxation time of the coarse-grained segment is shorter than the characteristic time of coarsening by constraint renewal. On the contrary, for bidisperse polymers in a certain time domain, CR-Rouse equilibration is slower than the coarsening of the segment, and hence the CR-Rouse mechanism dominates the relaxation.

In this work, we compare predictions of different slip-link simulations of bidisperse linear polymers to investigate the kinetics of $\{Z\}$ and $\{\mathbf{R}\}$. We choose Doi and Takimoto's (DT) model,[6] our primitive chain network (PCN) model,[5] and Nair and Schieber's (NS) model,[9] which differ in the implementation of constraint renewal. In the DT model, the $\{Z\}$ kinetics generates constraint renewal by direct (virtual) coupling among the chains, and new segments with new **R**-values are created by picking from a Gaussian distribution. In the NS model, constraint renewal is mimicked by Rouse-like fluctuations of $\{\mathbf{R}\}$ with a suitable diffusion coefficient, while $\{Z\}$ remains fixed. In our PCN model, the $\{Z\}$ kinetics of constraint renewal is somewhat equivalent to that of DT model, although $\{\mathbf{R}\}$ is changed by means of a force balance equation. Hence, a difference of the PCN model is that chain coupling at the nodes is effective (rather than virtual as in DT model), and the force balance in 3D space also accounts for a field force controlling density fluctuations, and for thermal fluctuations. The latter should not be confused with the **R**-fluctuations of the NS model.

In the following section, the models examined in this study are briefly summarized with the same notation for $\{\mathbf{R}\}$, $\{n\}$, $\{Z\}$, and other parameters. Comparison among the model predictions is then shown in subsequent sections. Constraint release as implemented in the PCN model will next be discussed after showing that it works successfully for bidisperse systems.

Models

DT Model. In the DT model,[6] many primitive path chains are created as random walks, with Z kinks per chain, the position of the kinks being indicated as $\{\mathbf{R}\}$. All kinks of the set of chains are coupled in pairs in a random way so as to account for constraint release (see below). Primitive chains are assumed to be embedded in the medium, so that the time evolution of $\{\mathbf{R}\}$ is simply described as (κ being the velocity gradient tensor):

$$\frac{\mathrm{d}\mathbf{R}_i}{\mathrm{d}t} - \kappa\cdot\mathbf{R}_i = 0 \tag{1}$$

Chain motion along the primitive path is 2-fold. Center of mass diffuses longitudinally to mimic reptation, and contour length L evolves according to the equation:

$$\frac{\mathrm{d}L}{\mathrm{d}t} = -\frac{1}{\tau_\mathrm{R}}(L - L_\mathrm{eq}) + \dot{L}_\mathrm{affine} + \sqrt{\frac{2a^2}{3\tau_0^\mathrm{DT} Z\Delta t}}\,g \tag{2}$$

In eq 2, L_eq is the mean equilibrium length, and the chain Rouse time τ_R is taken as $\tau_\mathrm{R} = \tau_0^\mathrm{DT} Z^2$, with τ_0^DT the unit time in the DT model. The term $\dot{L}_\mathrm{affine}$ is the change in L due to affine deformation of the medium. Finally, g is a Gaussian random term with zero mean and unit variance, a being the mean segment length of the equilibrium random walk, and Δt the time-step of numerical integration. Consistently with the above definition of Rouse time, the diffusion coefficient of the center of mass along the primitive path is given by $D = a^2/3\pi^2\tau_0^\mathrm{DT} Z$. Notice that the monomer number between kinks, $\{n_i\}$, does not appear explicitly in the DT model, because a uniform monomer density is assumed along the chain. Sliding of monomers through kinks is not described locally, but only focusing on the whole primitive chain (center of mass curvilinear diffusion plus L dynamics).

The number of kinks $\{Z\}$ is changed by motion of the chain ends, inducing constraint renewal. Indeed, when the length of a chain end becomes zero, the kink neighboring the chain end is removed. Simultaneously, the node coupled to the removed kink is also removed, thus mimicking constraint release. On the contrary, when the length of the chain-end segment becomes larger than a, a new node is created on it, and a random tangent vector is selected for the new end segment. At the same time, a new kink is created on another randomly selected segment, and coupled to the just created end kink, so as to mimic constraint creation. It should be noted that, because theory does not prescribe the position $\mathbf{R}$ of the new node on the "hooked" segment, several rules for its position in space were tested, and the results depended sensitively on such arbitrary choice. The rule was finally adopted to choose such position $\mathbf{R}$ randomly within a sphere of diameter a centered in the middle point of the hooked segment. The same algorithm for constraint renewal is also used by Likhtman.[8]

NS Model. In the NS model, the $\{\mathbf{R}\}$ dynamics is Rouse-like and hence accounts for local elastic forces acting along the chain and for stochastic forces representing constraint renewal. The equation of motion for $\{\mathbf{R}\}$ is then written as:

$$\frac{\mathrm{d}\mathbf{R}_i}{\mathrm{d}t} - \kappa\cdot\mathbf{R}_i = -\frac{a^2}{12kT\tau_\mathrm{CR}}\left(\frac{\partial F^\mathrm{NS}}{\partial \mathbf{R}_i}\right)_{T,\{n\},\{R_\mathrm{others}\}} + \sqrt{\frac{a^2}{6\tau_\mathrm{CR}\Delta t}}\,\mathbf{W} \tag{3}$$

Here, $\mathbf{W}$ is a random unit vector, and F^NS is the free energy of the chain, taken to be

$$F^\mathrm{NS} = F_\mathrm{e}(n_{i=1}) + \sum_{i=2}^{Z-1} F_\mathrm{s} + F_\mathrm{e}(n_{i=z}) \tag{4}$$

$$\frac{F_\mathrm{e}(n)}{kT} = -\frac{1}{2}\log(n) \tag{5}$$

$$\frac{F_\mathrm{s}}{kT} = \frac{3}{2}\frac{\mathbf{r}_i^2 n_0}{a^2 n_i} + \frac{3}{2}\log\left(\frac{2\pi n_i}{3}\right) \tag{6}$$

where n_0 is the average value of n_i at equilibrium, and $\mathbf{r}_i$ is the end-to-end vector of segment i. The characteristic times τ_CR in eq 3 determine the frequency of slip-link fluctuation due to constraint renewal and are assigned to nodes with a suitable

probability. The change of $\{Z\}$, as described below, also determines the τ_{CR} probability self-consistently.[9]

Sliding of monomers in the NS model is described through the following kinetic equation for $\{n\}$:

$$\frac{dn_i}{dt} = \frac{1}{kT\tau_i}(\mu_{i+1}^{NS} - \mu_i^{NS}) - \frac{1}{kT\tau_{i-1}}(\mu_i^{NS} - \mu_{i-1}^{NS}) + \sqrt{\frac{2}{\tau_i \Delta t}} W_i - \sqrt{\frac{2}{\tau_{i-1}\Delta t}} W_{i-1} \quad (7)$$

where $\tau_i = \tau_K(n_i + n_{i+1})/2n_0$ (with τ_K the Kuhn segment time), and W_i is a random flip ($W_i = 1$ or -1). The chemical potential μ_i^{NS} is obtained from the free energy shown in eqs 4−6.

Change of $\{Z\}$ is controlled in the following way. The probability to destroy the end node is assumed to be given by:

$$w_d = \frac{1}{n_0^2 \tau_K}\sqrt{\frac{3n_0}{n}} \quad (8)$$

Consistently with detailed balance, the probability to create a new node on the end segment is then obtained as:

$$w_c = \frac{1}{n_0^2 \tau_K}\sqrt{\frac{3}{nn_0}}(n-2) \quad (9)$$

Note that coupling among different chains is not considered in the NS model. Constraint renewal is accounted for in a mean-field way through diffusion of the nodes (the stochastic term in eq 3), somehow similarly to earlier molecular theories.[4,12,14,15] However, differently from those theories, the NS model makes no assumption on the factorability of the relaxation modulus.[12,14,15] In that respect, the NS model is closer to the theory proposed by Watanabe and Tirrell,[13] where the rate of constraint release depends on the configuration of the primitive path.

PCN Model. In the PCN model, the equation of motion for $\{\mathbf{R}\}$ is written as:

$$\frac{d\mathbf{R}_i}{dt} - \kappa \cdot \mathbf{R}_i = \frac{n_0}{2\tau_0^{PCN}} \sum_j^4 \frac{\mathbf{r}_j}{n_j} - \frac{n_0 a^2}{3kT\tau_0^{PCN}} \nabla_{\mathbf{R}} \mu^{PCN}(\mathbf{R}) + \sqrt{\frac{a^2}{2\tau_0^{PCN}\Delta t}} \mathbf{W}_i \quad (10)$$

The first term on the right-hand side is the sum of the elastic forces acting on the slip-link i. Differently from NS, where the free energy derivative accounts for two elastic forces, in the PCN model the elastic forces are those of the four strands belonging to the two chains coupled through the slip-link (entanglements are taken to be binary events). The second term is a field force generated by the chemical potential derived from a free energy F^{PCN}, reflecting repulsive interaction among the chain segments so as to maintain, to within small fluctuations, a uniform density. This free energy is written as

$$\frac{F^{PCN}(\mathbf{R})}{kT} = \begin{Bmatrix} \varepsilon\left(\frac{\phi(\mathbf{R})}{\langle\phi\rangle} - 1\right)^2 \text{for } \phi(\mathbf{R}) > \langle\phi\rangle \\ 0 \text{ for } \phi(\mathbf{R}) \le \langle\phi\rangle \end{Bmatrix} \quad (11)$$

where ϕ is the local segment density (evaluated in sub-boxes within the simulation box), and $\langle\phi\rangle$ is the average over the system (i.e., in the whole box). The numerical coefficient ε was fixed at 0.5. The last term in eq 10 accounts for thermal fluctuations of the slip-links. Note that such fluctuations are very different from those in the NS model. Indeed, the $\{\mathbf{R}\}$ fluctuation in the NS model mimics constraint renewal, and therefore τ_{CR} is of the order of the longest relaxation time of the chains. Conversely, in the PCN model, the $\{\mathbf{R}\}$ fluctuation is the local thermal motion of each node, and the time scale is given by $\tau_0^{PCN} = \zeta a^2/6kT$, where ζ is the subchain friction coefficient.

Time evolution of $\{n\}$ reflects the exchange of monomers between adjacent segments, i and $i-1$, and is written as:[5]

$$2\left(\frac{n_i}{r_i} + \frac{n_{i-1}}{r_{i-1}}\right)^{-1} \frac{dn}{dt} = \frac{n_0}{2\tau_0^{PCN}}\left(\frac{r_i}{n_i} - \frac{r_{i-1}}{n_{i-1}}\right) - \frac{n_0 a^2}{12kT\tau_0^{PCN}} \nabla_r \mu^{PCN} + \sqrt{\frac{a^2 n_0^2}{6\tau_0^{PCN}\Delta t}} W \quad (12)$$

The change of $\{Z\}$ in the PCN model occurs similarly to the DT model, with the important difference that the coupling between chains is not a virtual one. In the PCN model, the chain segment to be hooked is chosen randomly among neighboring segments within a distance of a from the hooking chain end. Also, the $\{n\}$ window at chain ends that triggers creation or destruction of an entanglement is somewhat different. At intervals of τ_0^{PCN}, monomers in chain ends are checked, and topology is preserved if n falls in the window:

$$0.5 < n/n_0 < 1.5 \quad (13)$$

In case of hooking ($n/n_0 \ge 1.5$), the position of the newly created node is automatically determined by the force balance expressed by eq 10.

Simulations

Simulations for the DT model were performed by using a code called PASTA, available on the web.[23] The calculation was made with 10 000 chains. $G^*(\omega)$ was obtained by the Fourier transform of the relaxation modulus for an initial shear strain of 0.5. Simulations for the PCN model were performed by our own code (named NAPLES) with a cell dimension of $(16a)^3$ with periodic boundary conditions and mean segment number density of $10/a^3$, corresponding to ca. 40 000 segments in the whole box. $G^*(\omega)$ was obtained from the stress response to sinusoidal shear deformations with a strain amplitude of 0.3. Results of the NS model were extracted from the literature,[9] where $G^*(\omega)$ is calculated (by using linear response theory) via the relaxation spectrum as obtained from equilibrium simulations.

Parameters

For each simulation, the parameters used to fit the experimental data are reported in Table 1. Slip-link models typically require a maximum of three parameters to fit calculation results to experimental data. They are as follows: (i) the molecular weight M_0 of the average chain segment at equilibrium (containing n_0 Kuhn segments), from which Z is determined as M/M_0, (ii) a modulus G_0, and (iii) a time τ_0, which, to within a numerical factor, is the Rouse time of the subchain (with molar mass M_0). In this Article, τ_0 is regarded as a best-fitting parameter, and we do not discuss it in detail.

It is known that there exists a model-dependent relation between G_0 and M_0.[25,26] For the DT model, such relation is written as:

Table 1. Parameters for the Simulations[a]

	polystyrene		polybutadiene	
model	G_0 (MPa)	M_0 (kDa)	G_0 (MPa)	M_0 (kDa)
NS	0.6*	18	4.6**	1.4
DT	0.75	14	3.2	2.0
PCN	0.33	11	1.8	1.6

[a] For the NS model, the value of G_0 was calculated from eq 14 with $^*\rho = 0.969$ g/cm^3 and $^{**}\rho = 0.826$ g/cm^3.[23,24]

$$G_0 = \frac{15}{4} G_N^{(0)} = 3\frac{\rho RT}{M_0} \tag{14}$$

Here $G_N^{(0)}$ is the plateau modulus, and ρ is the density of the sample. Equation 14 is widely used for tube-based constitutive equations and some slip-link models. Values of G_0 in Table 1 for the NS model were also calculated by using eq 14. On the other hand, for the PCN model the relation becomes:[27]

$$G_0 = \frac{\rho RT}{M_0} \tag{15}$$

Note that eq 15 is formally identical to, but physically different from, the well-known Ferry's relationship, because G_0 should not be confused with $G_N^{(0)}$.

To eliminate possible confusion on the use of either eq 14 or eq 15, both G_0 and M_0 are shown in Table 1, for each model and for each sample.

Results and Discussion

Figures 1 and 2 show predictions for $G^*(\omega)$ from DT, NS, and PCN models as compared to bidisperse data taken from the literature.[28,29] In both figures, the discrepancy shown by the DT model predictions at high frequencies is understandable because the DT model does not account for Rouse modes higher than the first, whereas it is not clear why the NS model shows a similar discrepancy in Figure 1. The range of low and intermediate frequencies requires a more thorough discussion.

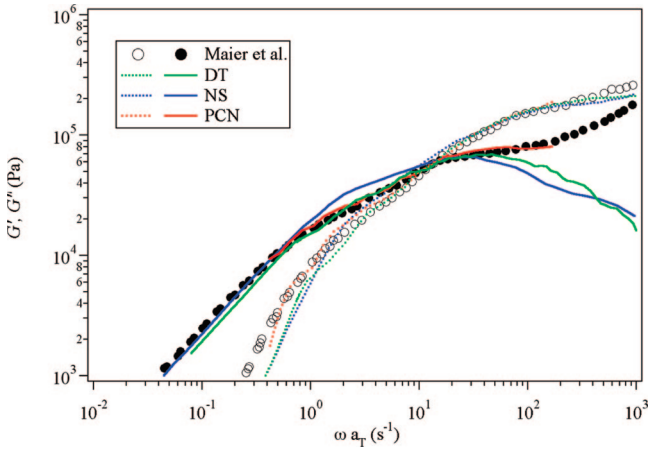

Figure 1. Predictions from different slip-link simulations for $G^*(\omega)$ of a bidisperse polystyrene melt with molecular weights of 177k and 60k, for a long-chain fraction of 0.6, at 170 °C.[28]

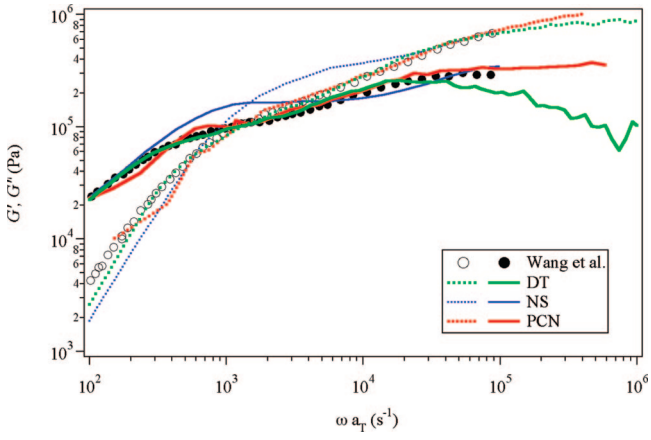

Figure 2. Predictions from different slip-link simulations for $G^*(\omega)$ of a bidisperse polybutadiene melt with molecular weights of 44k and 12k, for a long-chain fraction of 0.5, at 40 °C.[29]

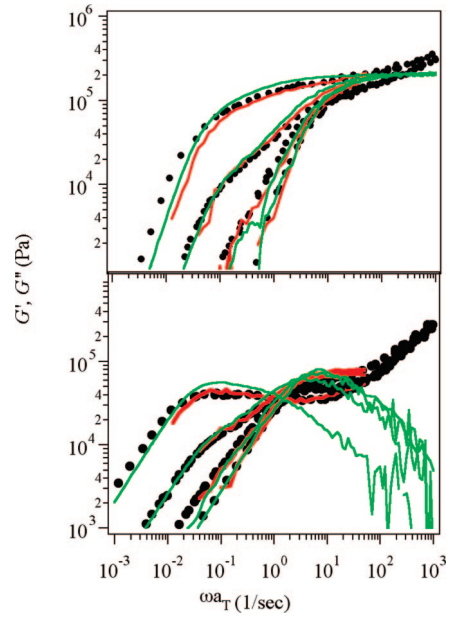

Figure 3. Predictions from DT (green lines) and PCN (red lines) simulations for $G^*(\omega)$ of bidisperse polystyrene melts with molecular weights of 294k and 83k at 167 °C.[30] The long-chain fraction is 0, 0.1, 0.4, and 1.0 from right to left.

In Figure 1, model predictions seem almost equivalent, although one may note that, in the intermediate frequency region, the G'' curve predicted by the NS model does not show the curvature change exhibited by both the data and the other simulations, and remains somewhat above the other curves. The molar mass ratio of the bidisperse system in Figure 1 is 177/60 $\approx$ 3, and hence, because the molecular weights of the two components are not very different, it is understandable that all models, which quantitatively predict monodisperse data, are also in reasonable agreement with the bidisperse ones.

Figure 2, on the other hand, emphasizes the peculiar behavior of NS model predictions barely visible in Figure 1. Indeed, in the intermediate region, NS model significantly overestimates the values of both moduli, whereas in the low frequency region G' appears somewhat underestimated. The molar mass ratio is here given by 44/12 $\approx$ 3.7, and hence it appears that the discrepancy sensitively increases with increasing dispersity.

It looks like the discrepancy is due to an inadequate description of constraint release for the longer chain through Rouse-like fluctuation of $\{\mathbf{R}\}$ at a rate controlled by the mean-field probability distribution of τ_{CR}. It is also known that an attempt of tuning the $\{\mathbf{R}\}$ dynamics by changing the number of chains involved in one entanglement (from 2 up to 5.4) was not effective.[9] On the other hand, such inexplicable inadequacy had been noted by the authors themselves.[9] In the following, we will focus on DT and PCN models only.

For further test on DT and PCN models, another experimental data set for bidisperse polystyrene melts[30] with several concentrations of the long chain was examined, and Figure 3 shows the results. Except for the discrepancy of the DT model in the high frequency region, accuracy of prediction is comparable for both models to within statistical error. A discrepancy is found for the case of pure long chains, where DT and PCN models predict a little faster relaxation than shown by the experiments, but the reason is unknown. All other data are quantitatively predicted without any concentration-dependent tuning parameter, that is, by using the same parameters (those in Table 1) for all curves. Hence, we may conclude that an adequate description for constraint renewal is the direct pairing employed in DT and PCN models.

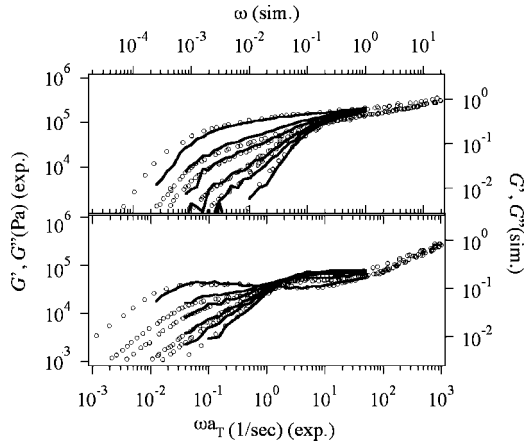

Figure 4. Predictions from PCN simulations (solid lines) for the same experimental data of Figure 3 (○) at long-chain fractions of 0, 0.1, 0.2, 0.4, 0.6, and 1.0 from right to left.

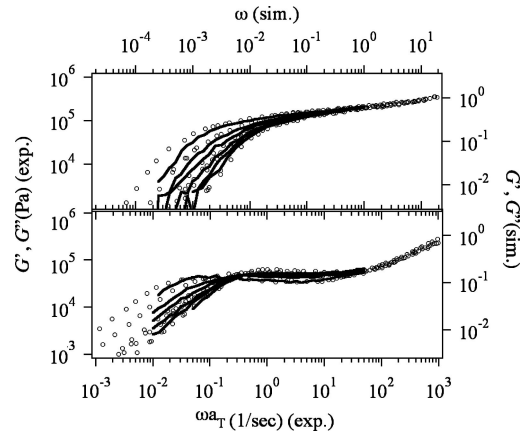

Figure 5. Same as in Figure 4 for molecular weights of 294k and 161k at 167 °C.[30]

Additional results for the PCN model only, again with the same set of polystyrene parameters, are shown in Figures 4 and 5. (Data in Figure 4 are partly the same for Figure 3.) Clearly, the PCN model quantitatively predicts the experimental data.

The agreement of DT and PCN with experiments indicates that these models reasonably reproduce the competition between DTD and CR-Rouse dynamics. It is also noted that the Struglinski−Graessley parameter[31] of the bidisperse melts examined in this study is much smaller than the critical value of 0.5 (0.01 for the DT model and 0.05 for the PCN model in Figure 3, for example). Hereafter, we further discuss the competition between DTD and CR-Rouse for what concerns the PCN model only.

For a discussion on DTD coarsening, Figure 6 shows time evolution of the fraction of surviving nodes on long chains, for the case of 10% long-chain concentration (one of the data in Figures 3 and 4). The normalized storage modulus of the long-chain fraction is also plotted for comparison. The surviving node fraction (solid curve) shows a clear shoulder due to the different relaxation behavior of nodes composed by long−short chains from those made of long−long ones, whereas the relaxation modulus (circles) falls down smoothly, without showing any shoulder. Such a contrast implies that, in the time domain of the shoulder, the relaxation modulus is controlled by CR-Rouse dynamics rather than by DTD. The delay in relaxation as compared to DTD coarsening has also been observed experimentally.[21]

Superimposed snapshots of a long chain (one every 10 time units) are shown in Figure 7, thus providing a visual image of

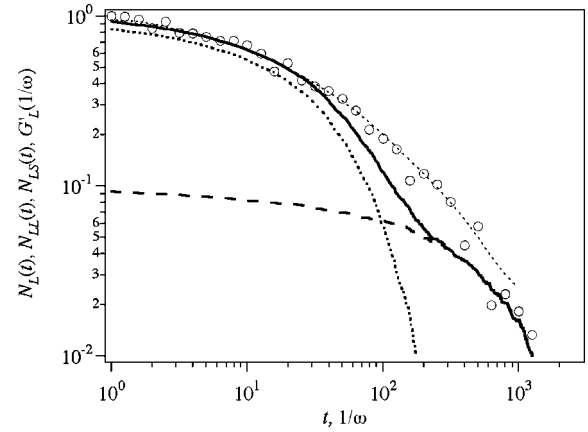

Figure 6. Fraction of surviving nodes on long chains from the PCN simulations used for the results reported in Figures 3 and 4 at a long-chain concentration of 10%. The solid curve indicates the total survival fraction on long chains, $N_L(t)$, the broken curve refers to long−long entanglements only, $N_{LL}(t)$, and the dotted curve refers to long−short entanglements, $N_{LS}(t)$. The ○ show the normalized storage modulus of the long-chain portion plotted against $1/\omega$, with an eye guide for easy comparison.

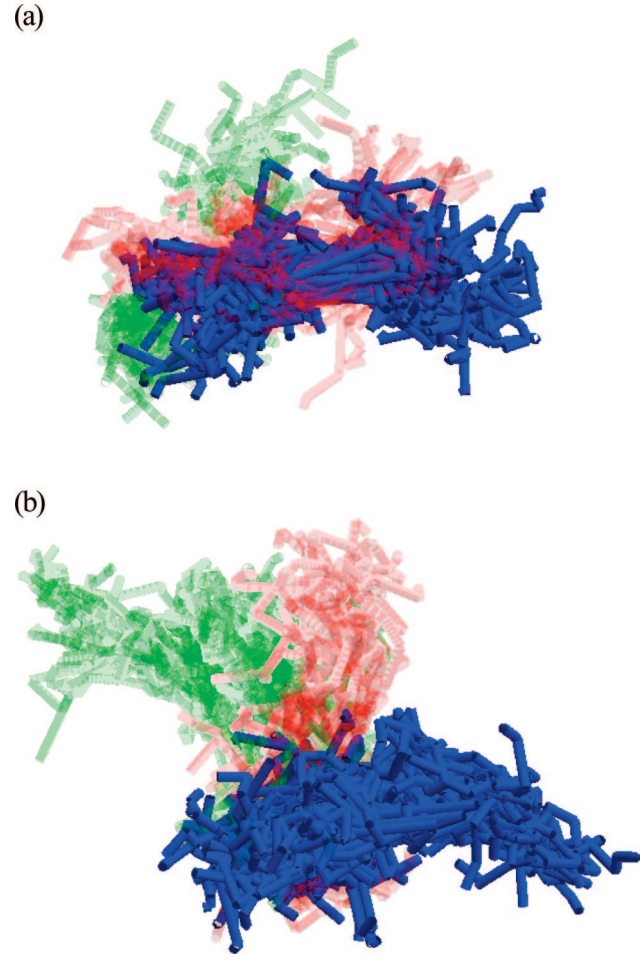

Figure 7. Superimposed snapshots (taken every 10 time units) of chain conformation from the PCN simulations for a long-chain fraction of 1.0 (a) and 0.1 (b) used for the results shown in Figures 3 and 4. Each color indicates a sequence of 100 time units.

the long-chain dynamics. As for the different colors, each covers 100 time units, a time span over which we know (see Figure 6) that the short chains have renewed all entanglements. Thus, the "thickness" of each color provides a visual image of the lateral fluctuations of the long chains over 100 time units. Comparing

such thickness for the 100% long-chain melt in Figure 7a to that for the 10% long-chain blend in Figure 7b, it is noted that such thickness is not much larger for the blend case, confirming the information provided by Figure 6 that DTD does not dominate. Notice, however, that the lateral fluctuations are not due only to constraint release, as thermal fluctuation of the entangled network is also included.

The different colors, ordered as blue−red−green, correspond to 300 consecutive time units in total. Over such a longer time, a much larger difference is found between Figure 7b, for the concentration of 0.1, and Figure 7a for the pure long-chain melt; for example, the rotational relaxation of the primitive path is significantly accelerated in Figure 7b. The rotational relaxation corresponds to dielectric relaxation for type-A polymers,[22] and according to the relation to viscoelastic relaxation,[22] acceleration of viscoelastic relaxation can be also obtained. This is consistent with the fact that the stress contributed by the long chains drops to ca. 10% of the initial value over 300 time units in the blend case (see top curve in Figure 6), while the drop is by less than a factor of 2 in the pure melt case (see the $N_{LL}(t)$ curve in Figure 6).

For sake of completeness, it may be worth mentioning one possible additional effect of constraint release called "enhanced reptation" by Hua and Ke.[18] The idea is that constraint renewal, by suppressing or creating kinks in the primitive path, changes the path length and hence enhances the rate of path-length fluctuations. In the lattice simulations of Hua and Ke, the effect was present, and they found good agreement with bidisperse data. The same effect is certainly present also in the DT model simulations through sudden change of L in eq 2, and in the PCN model in an indirect way, that is, through force balance on nodes and monomer sliding through slip-links.

Conclusions

Slip-link simulations for bidisperse polymer melts made by using the Doi and Takimoto (DT) model, the Nair and Schieber (NS) model, and the PCN model by Masubuchi et al. were examined to discuss the effect of constraint release, which is accounted for differently in each model. It was found that the mean-field NS model is inferior to the other two models for the case of bidisperse melts where the molecular weights of the components are well separated. The reason is unknown, except for the obvious consideration that a mean-field approach captures local interaction effects less effectively than do models embodying chain coupling explicitly.

Further tests were performed on DT and PCN models against data with varying long-chain concentration, which showed quantitative agreement of simulation predictions with the experimental data. Analysis on the lifetime of entanglement nodes and visualization of fluctuations in the PCN model indicates that the competition between CR-Rouse and DTD relaxations is reasonably accounted for. Further test of the models is needed against other experimental data, such as those involving dielectric relaxation. Because the simulations for the existing data in the literature are time-consuming due to the large molecular weights used in the experiments, such results will be reported in a future publication.

Acknowledgment. We thank Professor J. D. Schieber for providing his simulation data and for useful discussions. We also thank Professor J.-I. Takimoto for allowing us to use his PASTA code and for helpful comments. This work was partly supported by CREST and PRESTO by Japan Science and Technology Agency, and by the Ministry of Education, Science, Sports and Culture, Grant-in-Aid for Scientific Research (B), 20340111, 2008.

References and Notes

(1) Hua, C. C.; Schieber, J. D. *J. Chem. Phys.* **1998**, *109*, 10018.
(2) Green, M. S.; Tobolsky, A. V. *J. Chem. Phys.* **1946**, *14*, 80.
(3) Doi, M.; Edwards, S. F. *The Theory of Polymer Dynamics*; Oxford University Press Inc.: Clarendon, 1986.
(4) Graessley, W. W. *Adv. Polym. Sci.* **1982**, *47*, 68.
(5) Masubuchi, Y.; Takimoto, J.-I.; Koyama, K.; Ianniruberto, G.; Marrucci, G.; Greco, F. *J. Chem. Phys.* **2001**, *115*, 4387.
(6) Doi, M.; Takimoto, J.-I. *Philos. Trans. R. Soc. London, Ser. A* **2003**, *361*, 641.
(7) Schieber, J. D.; Neergaard, J.; Gupta, S. *J. Rheol.* **2003**, *47*, 213.
(8) Likhtman, A. E. *Macromolecules* **2005**, *38*, 6128.
(9) Nair, D. M.; Schieber, J. D. *Macromolecules* **2006**, *29*, 3386.
(10) Tsenoglou, C. *Polym. Prepr. (Am. Chem. Soc., Div. Polym. Chem.)* **1987**, *28*, 185.
(11) des Cloizeaux, J. *J. Europhys. Lett.* **1988**, *5*, 437.
(12) Rubinstein, M.; Colby, R. H. *J. Chem. Phys.* **1988**, *89*, 5291.
(13) Watanabe, H.; Tirrell, M. *Macromolecules* **1989**, *22*, 927.
(14) Pattamapron, C.; Larson, R. G. *Rheol. Acta* **2001**, *40*, 516.
(15) Likhtman, A. E.; McLeish, T. C. B. *Macromolecules* **2002**, *35*, 6332.
(16) Graham, R. S.; Milner, S. T.; Likhtman, A. E.; McLeish, T. C. B. *J. Rheol.* **2003**, *47*, 1171.
(17) Leygue, A.; Bailly, C.; Keunings, R. *J. Non-Newtonian Fluid Mech.* **2006**, *136*, 1.
(18) Hua, C. C.; Ke, C. C. *J. Polym. Res.* **2005**, *12*, 181.
(19) Marrucci, G. *J. Polym. Sci., Polym. Phys. Ed.* **1985**, *23*, 159.
(20) Orwoll, R. A.; Stockmayer, W. H. *Adv. Chem. Phys.* **1969**, *15*, 305.
(21) Watanabe, H.; Ishida, S.; Matsumiya, Y.; Inoue, T. *Macromolecules* **2004**, *37*, 6619.
(22) (a) Watanabe, H. *Prog. Polym. Sci.* **1999**, *24*, 1253. (b) Watanabe, H. *Macromol. Rapid Commun.* **2001**, *22*, 127, and references therein.
(23) http://octa.jp.
(24) Fetters, L. J.; Lohse, D. J.; Richter, D.; Witten, T. A.; Zirkel, A. *Macromolecules* **1994**, *27*, 4639.
(25) Masubuchi, Y.; Ianniruberto, G.; Greco, F.; Marrucci, G. *J. Chem. Phys.* **2003**, *119*, 6925.
(26) Larson, R. G.; Sridhar, T.; Leal, L. G.; McKinley, G. H.; Likhtman, A. E.; McLeish, T. C. B. *J. Rheol.* **2003**, *47*, 809.
(27) Masubuchi, Y.; Ianniruberto, G.; Greco, F.; Marrucci, G. J. *Non-Newtonian Fluid Mech.* **2008**, *149*, 87.
(28) Maier, D.; Eckstein, A.; Friedrich, Cr.; Honerkamp, J. *J. Rheol.* **1998**, *42*, 1153.
(29) Wang, S.; von Meerwall, E. D.; Wang, S.-Q.; Halasa, A.; Hsu, W.-L.; Zhou, J. P.; Quirk, R. P. *Macromolecules* **2004**, *37*, 1641.
(30) Watanabe, H.; Sakamoto, T.; Kotaka, T. *Macromolecules* **1985**, *18*, 1008.
(31) Struglinski, M. J.; Graessley, W. W. *Macromolecules* **1985**, *18*, 2630.

MA800954Q